Sulfonated silica-based cation-exchange nanofiber membranes with superior self-cleaning abilities for electrochemical water treatment applications

Bianca Swanckaert[a], Eva Loccufier[a], Jozefien Geltmeyer[a], Korneel Rabaey[b,c], Klaartje De Buysser[d], Luiza Bonin[b,c,*], Karen De Clerck[a,*]

[a] *Centre for Textile Science and Engineering (CTSE), Department of Materials, Textiles and Chemical Engineering (MaTCh), Faculty of Engineering and Architecture Ghent University, Technologiepark 70a, 9052 Ghent, Belgium*

[b] *Center for Microbial Ecology and Technology (CMET), Department of Biotechnology, Faculty of Bioscience Engineering Ghent University, Coupure Links 653, 9000 Ghent, Belgium*

[c] *Center for Advanced Processes and Technology for Urban Resource recovery (CAPTURE), Frieda Saeysstraat 1, 9000 Ghent, Belgium*

[d] *Sol-gel Centre for Research on Inorganic Powders and Thin Films (SCRiPTS), Department of Chemistry, Faculty of Sciences Ghent University, Krijgslaan 281 S3, 9000 Ghent, Belgium*

* Corresponding authors: Karen De Clerck (Karen.DeClerck@UGent.be), Luiza Bonin (Luiza.Bonin@UGent.be)

ABSTRACT

Electrochemical treatments in (waste)water management show high potential in the global water resource crisis, but are often limited by the ion-exchange membrane (IEM) performance. Low chemical resistance and fouling are major issues in the development of next-generation IEMs. Sulfonated silica-based nanofiber cation-exchange membranes (CEMs) offer a promising solution to these issues due to their superior chemical resistance and self-cleaning properties. Via the direct electrospinning of a sol-gel solution starting from tetraethyl orthosilicate (TEOS) and 3-mercaptopropyl triethoxysilane (MPTES), nanofiber membranes with an ion-exchange capacity (IEC) of 1.3 mmol g^{-1} can be produced without the need of an additional matrix. The produced nanofiber CEM performs excellent in lab-scale electrochemical tests, with a resistance of $3.2 \pm 0.4 *10^{-3}$ Ω m² and a Coulombic efficiency of $\pm 70\%$ for the transport of Na^+ using a current density of either 128 or 256 A m^{-2}. Furthermore, the nanofiber CEM shows outstanding resistance against strong acidic solutions and chlorine. After fouling of the membrane with $CaCO_3$, the nanofiber CEM shows self-cleaning properties, eliminating the need for an additional cleaning step during usage. These results illustrate the excellent performance of the silica-based nanofiber CEM for industrial water treatment applications.
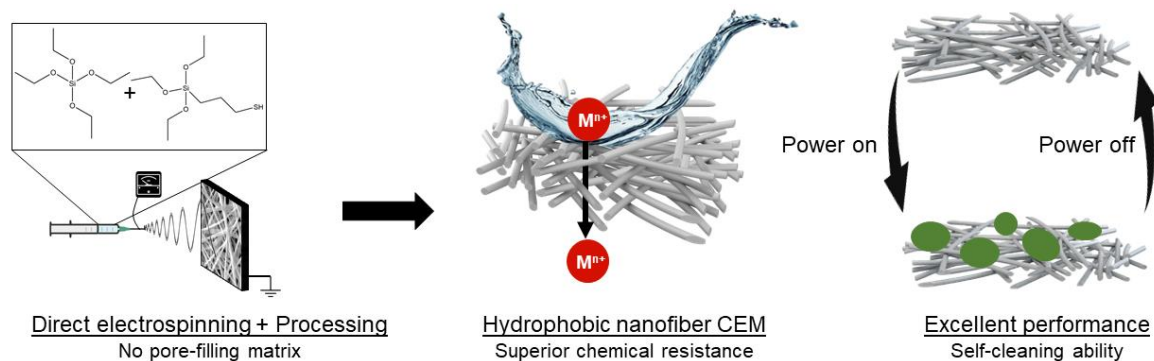
KEYWORDS

Silica nanofibers, cation-exchange membrane, self-cleaning, fouling, electrochemical water treatment

HIGHLIGHTS

- Sulfonated silica-based cation-exchange nanofibers were electrospun for the first time
- No additional matrix required; use of nanofibers as porous CEM
- The silica-based nanofiber CEM has an excellent chemical resistance
- The silica-based nanofiber CEM showcases performance in line with the commercial CMI-7000 CEM
- The silica-based nanofiber CEM has self-cleaning properties after fouling

GRAPHICAL ABSTRACT

Direct electrospinning + Processing
No pore-filling matrix

Hydrophobic nanofiber CEM
Superior chemical resistance

Power on · Power off

Excellent performance
Self-cleaning ability

1. INTRODUCTION

In battling the global water resource and energy crisis, electrochemical water treatment systems are deployed as promising techniques for i.e. disinfection of wastewater, resource recovery and energy production [1]–[6]. Optimizing these electrochemical processes is of utmost importance to tackle the ongoing water shortages and the depletion of available resources worldwide. For optimal efficiency, these processes use an ion-exchange membrane (IEM) that separates the anolyte and catholyte compartments. IEMs can typically be divided into two categories: cation-exchange membranes (CEM) that allow passage of cations and consist of negatively charged functional groups such as $-SO_3^-$, $-COO^-$, $-PO_4^{2-}$; and anion-exchange membranes (AEM) that allow passage of anions and contain positively charged functional groups such as $-NR_3^+$, $-NHR_2^+$ [7]–[10]. These membranes must meet some very challenging demands, namely high chemical resistance, mechanical stability, excellent water barrier properties, good ion affinity and transport, high permselectivity and low electrical resistance [10]–[13]. Over the past decades, extensive research has been performed in developing stable, optimal IEMs for fuel cell applications. Recently, the use of IEMs in water treatment applications has been explored as well and often requires more strict membrane demands such as good fouling resistance [12], [14]. Current commercial membranes still suffer considerably from fouling and scaling during usage, requiring extensive and expensive cleaning processes, via acid/alkaline treatment or polarity reversal [15], [16]. This can significantly damage the membranes and/or reduce industrial efficiency [17]–[26]. Additionally, many CEMs still consist of fluorinated components, which should be eliminated in view of today's environmental challenges. Therefore, there is an urgent need for new membranes that show excellent chemical resistance and, more specifically, improved fouling properties and/or cleaning efficiency. These new IEMs should show beneficial properties for water treatment applications but could be applied in a broader field as well, such as fuel cells and heavy metal ion removal.

An interesting new development is the use of nanofibers in IEMs. Nanofibers typically have a submicron diameter with values even as low as 50 nm and are generally produced via a process called electrospinning [27], [28]. Electrospinning allows for the creation of non-woven membranes made of nanofibers. These nanofibers are commonly made from organic polymers and are often incorporated in a pore-filling matrix to enhance the mechanical stability of the IEM [29]. Nanofibers have been shown to improve the resistance and fouling of membranes [30]–[33]. Additionally, their specific morphology results in a high surface area with various accessible surface groups which can be tuned for optimal ion transport. The specific surface area increases with decreasing fiber diameter, and the ionic properties increase exponentially [33]–[36]. However, these organic membranes often show relatively poor chemical stability, and the presence of the pore-filling matrix often restricts the superior effect of the nanofiber morphology on their ionic properties [33], [37]. These issues limit the industrial potential of the organic nanofiber IEMs. Ceramic nanofibers as IEMs can offer a promising solution. They combine the extraordinary properties of both ceramic and nanofibrous materials, resulting in a high thermal and chemical resistance and a porous and flexible structure with a high surface area [38]–[41]. Traditionally, ceramic nanofibers are produced with the aid of a sacrificing polymer to control the rheological properties during electrospinning. This polymer is then removed by a thermal treatment, resulting in pure ceramic nanofibers [42]. However, this process results in rough and uneven fibers with poor coherence, resulting in poor mechanical properties [43], [44]. Direct electrospinning of ceramic nanofibers (without the need of a sacrificing polymer) is more challenging but allows for dense, mechanically strong and tuneable nanofibers that can be used as membrane structures [44], [45]. Our earlier work showed the successful

88 electrospinning of silica nanofibers, starting from a sol-gel synthesis of TEOS without the need for the
89 addition of an organic polymer. This is done by carefully controlling the molar ratios and reaction time
90 during the synthesis, resulting in a stable sol which can be electrospun for multiple hours and this results
91 in stable, less brittle, upscalable structures [44], [45]. This is thus the preferred method.

92 In this research, ceramic nanofibers made from silica, produced via a combination of sol-gel synthesis
93 and direct electrospinning, are developed for ion-exchange. This silica membrane allows for a simple
94 functionalization due to the presence of reactive hydroxyl groups on the surface of the fibers. This offers
95 opportunities to tune the material's properties given a wide range of challenging applications [46]. This
96 work focuses on the functionalization of the silica nanofiber structure towards a cation conductive
97 membrane via a straightforward method as inspired by Cano-Serrano *et al.*, who produced sulfonic acid
98 functionalized silica gels through the oxidation of thiol groups [47]. It is known that electrospinning
99 charged systems can be very challenging and unstable [29]. Therefore, a thiol-functionalized silica
100 system was first electrospun into nanofibers and oxidized afterwards to obtain sulfonic acid-
101 functionalized silica nanofibers. As such, the production of a ceramic silica-based nanofiber CEM is
102 illustrated for the first time, via a direct electrospinning process of a solution produced by the co-
103 condensation of tetraethylorthosilicate (TEOS) and 3-mercaptopropyl triethoxysilane (MPTES)
104 precursors (Figure 1). Additional focus is given to the functionalization of the silica-based membrane
105 with hydrophobic alkyl chains, using chlorosilanes and the reactive hydroxyl groups on the silica
106 structure, to obtain a separation membrane. As a result, the produced non-fluorinated nanofiber
107 membrane in this work can be used as porous CEM without the need for an additional matrix material.
108 This is in contrast to most ongoing research on ion-exchange nanofibers, where the produced nanofiber
109 mat is post-treated into a dense membrane by the addition of a pore-filling matrix. This composition
110 usually restricts the ionic properties of the nanofibers, and as such, the outstanding performance of the
111 nanofibers is not fully exploited [29]. By producing a water-repellent ion-exchange nanofiber membrane,
112 the desired nanofiber morphology is retained, while separation is still assured. This novel membrane
113 was tested in a lab-scale electrochemical cell (EC) to determine its performance in electrochemical water
114 treatment applications as well as its fouling stability, which is often a major issue for common
115 membranes. A commonly used non-fluorinated, dense, commercial membrane, namely CMI-7000
116 (Membranes International Inc., USA), which has a high robustness, was used as a reference to set a
117 target value for industrial performance. This work demonstrates that the porous nanofiber CEM already
118 shows an excellent performance compared with the dense CMI-7000 reference, with superior fouling
119 performance and self-cleaning abilities, which allows for the elimination of energy-intensive cleaning
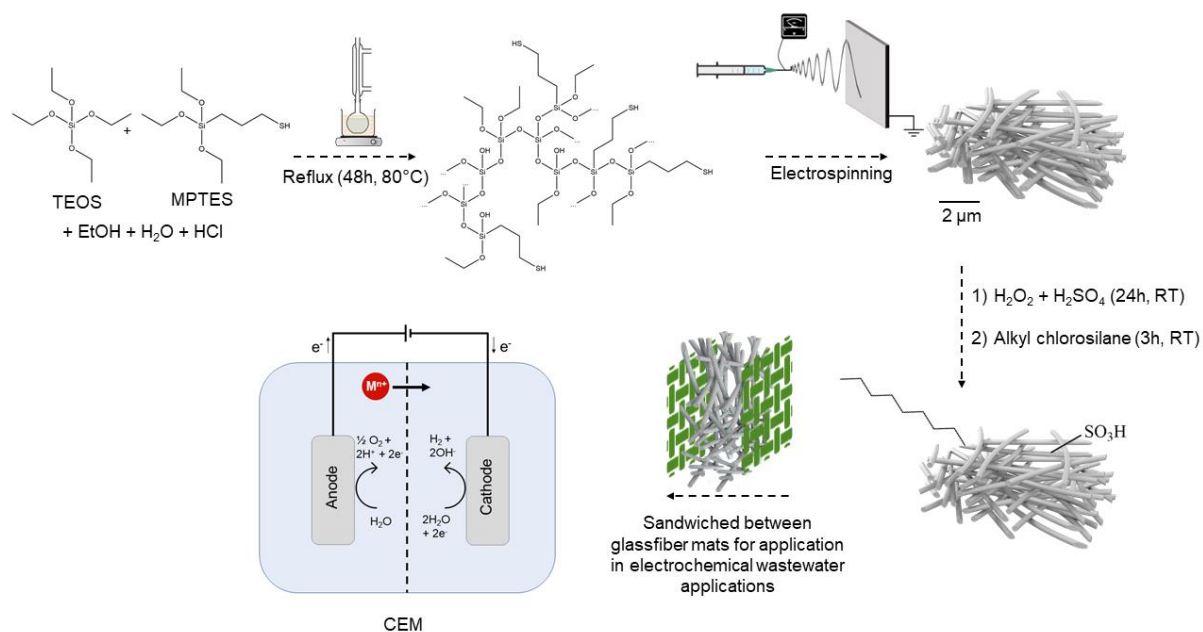120 and/or polarity reversal steps in industrial applications.

121

122 Figure 1: Overview of the production process of silica-based nanofiber CEM. By co-condensation of TEOS and MPTES, a thiol-
123 functionalized network is obtained and electrospun into nanofibers. Further oxidation of the thiol groups results in sulfonated

124 nanofibers. To ensure the water-repellent properties of the silica-based nanofiber CEM, they are functionalized with hydrophobic
125 alkyl chains using chlorosilanes.

2. MATERIALS AND METHODS

2.1 Materials

For the membrane production TEOS (≥ 99%), MPTES (≥ 80%), hydrochloric acid (HCl, 37%), hydrogen peroxide (H_2O_2, 30%) and chloro-trihexylsilane (Cl-THS, 97%) were purchased from Sigma Aldrich. Ethanol (EtOH, ≥ 99.8%) was obtained from VWR. Chloro-triethylsilane (Cl-TES, ≥ 98%) and chloro-tributylsilane (Cl-TBS, 97%) were purchased from Alfa Aesar. Chloro-butyldimethylsilane (Cl-BdMS, 97%), chloro-hexyldimethylsilane (Cl-HdMS, 97%), chloro-octyldimethylsilane (Cl-OdMS, 97%) were obtained from ABCR and chloro-trimethylsilane (Cl-TMS, 98%) was obtained from Acros Organics. The glass fiber woven support (25 g m^{-2}) was purchased from EasyComposites. For the membrane testing sodium chloride (NaCl, ≥ 99%), sodium sulfate (Na_2SO_4, ≥ 99%), Sodium phosphate (NaH_2PO_4, ≥ 99%), lithium sulfate (Li_2SO_4, ≥ 98.5%), potassium sulfate (K_2SO_4, ≥ 99%), potassium carbonate (K_2CO_3, ≥ 99%) and calcium nitrate ($Ca(NO_3)_2$, ≥ 99%) were purchased from Sigma Aldrich. CMI-7000 (Membranes International Inc., USA) was used as a reference CEM.

2.2 Methods

Electrospinning and functionalization of silica-based nanofiber CEM

The silica-based nanofiber CEM was produced by modifying the procedure for pure silica nanofibers developed by Choi *et al.* and optimized by Geltmeyer *et al.* [44], [48]. Nanofibers were produced starting from a solution of TEOS, MPTES, ethanol, distilled water and HCl with molar ratios of 1:x:2:y:0.01 respectively, with x and y varied from 0.1 to 0.4 and 2 to 3, respectively, to obtain an optimal electrospinning process with a maximized MPTES loading. TEOS and MPTES were first mixed with ethanol, and aqueous HCl was added dropwise while stirring. Afterwards, the solution was heated at 80°C in a reflux setup. After 48h the reflux was removed and the reaction was continued under atmospheric conditions until a viscosity between 150 and 200 mPa s was reached. The viscosity was measured using a Brookfield viscometer LVDV-II. Electrospinning was done on an in-house developed rotating drum collector with a high-voltage source from Glassman high voltage inc. and a pump from kdScientific. Stainless steel needles were used with an inner diameter of 0.8 mm. The flow rate was set at 1 mL h^{-1}, the tip-to-collector distance at 15 cm and the voltage was set between 20 and 25 kV for a stable electrospinning process. Nanofiber membranes with a surface density of ± 40 g m^{-2} were produced. The obtained nanofiber membranes were oxidized by immersing them for 24h at room temperature (RT) in 100 mL of a 30% H_2O_2 solution with ± 5 droplets of H_2SO_4 added. They were rinsed afterwards with an excessive amount of deionized water. This resulted in the conversion of -SH into -SO_3H [49]. Additionally, to obtain a hydrophobic membrane, the cation-exchange nanofiber membranes were immersed in solutions of different chlorosilanes for 3h at RT and were rinsed extensively with ethanol afterwards.

Characterization of the silica-based nanofiber CEM

The morphology of the nanofibers was examined with a Phenom Tabletop SEM XL. ATR-FTIR spectra were recorded with a Nicolet iS50 FT-IR setup within the range of 400-4000 cm^{-1}. Additionally, the porosity (ε) was calculated via Eq. (1).

$$\varepsilon \ (\text{-}) = 1 - \frac{m/\rho}{l\,b\,t} \qquad (1)$$

With m the mass of the nanofiber membrane, ρ the density of the nanofiber membrane (set at the value for pure dense amorphous silica (2.2 g cm^{-3})), l, b and t are the length, width and thickness of the membrane, respectively, and were measured with a micrometer. The theoretical average pore size diameter and specific surface area of the nanofibers were calculated using the work of Eichhorn *et al.* [50]. Ion-exchange capacity (IEC) measurements were performed by immersing the samples in 1 mol.L^{-1} NaCl solutions for at least 24h during which H^+ on the membrane is exchanged with Na^+ from the solution. Afterwards, the amount of exchanged H^+ was measured by an acid-base titration with 0.01 mol.L^{-1} NaOH. The IEC was calculated according to Eq. (2).

4

173
$$\text{IEC (mmol g}^{-1}) = \frac{c_{NaOH} V_{NaOH}}{m} \qquad (2)$$

174 With c_{NaOH} the concentration of NaOH, V_{NaOH} the titrated volume and m the mass of the membrane. The
175 water uptake was measured by immersing the membranes in H_2O for 24h at RT. Afterwards, the surface
176 water was removed and the wet mass was determined (W_{wet}). The membranes were dried and their dry
177 mass was determined (W_{dry}). The water uptake was calculated according to Eq. (3).

178
$$\text{WU (\%)} = \frac{W_{wet} - W_{dry}}{W_{dry}} \qquad (3)$$

179 The XPS and sputter-profiling experiments were carried out in UHV on an ESCALAB (VG Scientific)
180 spectrometer. XPS spectra were recorded using an Al Kα(1486.6 eV) X-ray source. A low-energy
181 electron flood gun of 3 eV was used as a neutralizer. The samples were analyzed using a nickel grid to
182 minimize peak distortion due to charging. All peak deconvolution is performed with Shirley background
183 subtraction and a mixed Gaussian/Lorentzian symmetrical peak shape using Casa XPS software and
184 sensitivity factors as provided within the software. Peak positions were calibrated towards a value of
185 284.6 eV for the C1s peak for adventitious carbon. Water contact angle (WCA) measurements were
186 performed with optical contact angle measurement and drop analysis at RT (Dataphysics Instruments).
187 For each sample, 10 measurements were done after the droplets were stabilized (< one minute) and
188 the average was taken. Mechanical properties were determined with a DMA Q800 (loadcell 18 N, strain
189 rate 1 % min^{-1}). Per test, 3 samples were measured. The samples had a gauge length of 2 cm and a
190 width of 0.7 cm. The cross-section was calculated based on the mass and density of the samples. Both
191 dry and wet samples were tested, with the wet samples being immersed in 1 mol.L^{-1} NaCl for at least
192 24h. Thermal resistance was tested with thermogravimetric analysis (TGA) (Netzsch STA 409 PC) with
193 a temperature increase of 10°C min^{-1} until 900°C in air.

194 *Performance of the silica-based nanofiber CEM*

195 A lab-scale EC made of plexiglass was used (12x8 cm). The EC consisted of two compartments
196 separated by the nanofiber membrane sandwiched between glass fiber woven support, or CMI-7000,
197 respectively (8x1 cm). A titanium plate with mixed metal oxide (MMO) coating was used as the anode;
198 a stainless steel mesh was used as the cathode. Rubber sheet seals were sandwiched between the
199 compartments to avoid leakage, and the compartments were bolted together (Figure 2). The lab-scale
200 reactor was then connected to a power supply (AIM TTi PL601 of 60 V and 1.5 A).
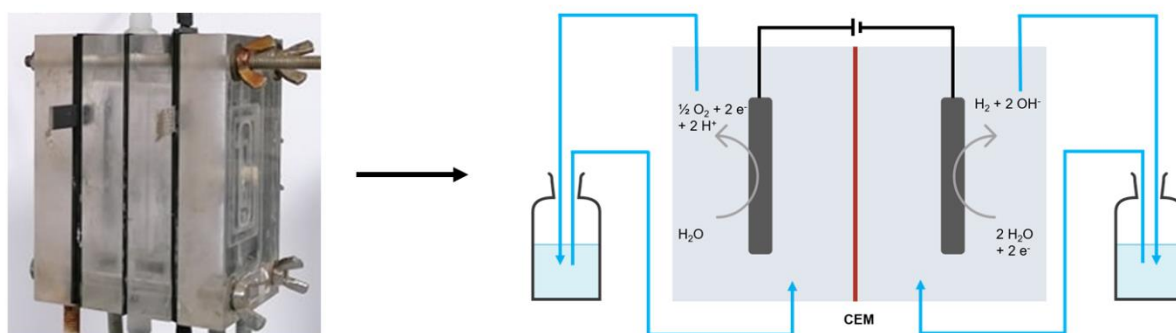
201

202 Figure 2: Lab-scale EC setup made from plexiglass with two compartments separated by a cation-exchange membrane.

203 For all tests, the samples were first immersed in 1 mol.L^{-1} NaCl for 24h as pre-treatment. The membrane
204 resistance was determined by a current interrupted (iR) test with a 1 mol.L^{-1} NaCl solution at both anolyte
205 and catholyte. A VSP Multi Potentiostat (Bio-Logic Science Instruments SAS, Claix, France) was used
206 to perform the iR tests. A three electrode system was used with the working electrode at the cathode,
207 and two Ag/AgCl reference electrodes placed at the cathodic and anodic compartment consecutively. A
208 current density of 256 A m^{-2} was applied for 2 s, followed by an interruption of 0.2 s. This was repeated
209 for 10 cycles and the average resistance was calculated from the change in potential. When the
210 reference electrode was placed at the cathodic compartment, the resistance of the solution was
211 measured (R_s). When the reference electrode was placed at the anodic compartment, the resistance of

212 the solution and membrane was measured (R_{s+m}). The membrane resistance (R_m) was then calculated
213 via Eq. (4).

$$R \text{ } (\Omega \text{ m}^2) = (R_{s+m} - R_s) * A \tag{4}$$

215 With A the surface area of the membrane, which equals $8*10^{-4}$ m² is this research.

216 The Coulombic efficiency (CE) was determined by performing ion migration tests for 48h with 1 mol.L^{-1}
217 Na$_2$SO$_4$ at both 128 and 256 A m^{-2}. Na$^+$ concentration at both anolyte and catholyte was assessed by
218 ion chromatography (IC) measurements (Metrohm AG, Herisau, Switzerland). From these
219 measurements the CE could be determined by Eq. (5).

$$CE \text{ } (\%) = 100 * \frac{(n_t - n_0) \text{ } z \text{ } F}{I \text{ } t} \tag{5}$$

221 With $n_t - n_0$ the amount of Na$^+$ (in moles) that migrated determined via IC, z is the valence of the cations,
222 F is the Faraday constant, I the current and t the time (48h).

223 The permselectivity was determined after 48h by calculating the selectivity number via Eq. (6).

$$\text{Selectivity number (-)} = \frac{n_{Na^+}}{n_{Na^+} + n_{SO_4^{2-}}} \tag{6}$$

225 With n_{Na^+} the amount of Na$^+$ that migrated after 48h and $n_{SO_4^{2-}}$ the amount of SO_4^{2-} that migrated after
226 48h.The energy consumption (E_c) during ion migration was calculated via Eq. (7).

$$E_c \text{ } (Wh \text{ } g^{-1}) = \frac{I \text{ } V \text{ } t}{m_{Na}} \tag{7}$$

228 With I the current, V the voltage, t the time (in this research 48h) and m_{Na} the amount of Na$^+$ that migrated
229 after 48h. The selectivity of the membranes was determined by doing an ion migration test with 0.25
230 mol.L^{-1} of Na$_2$SO$_4$, Li$_2$SO$_4$ and K$_2$SO$_4$ at 128 A m^{-2}. IC measurements determined the concentration of
231 cations at both anolyte and catholyte over time. The chemical resistance was first determined ex-situ by
232 immersing membrane samples in solutions of 1, 2 and 3 mol.L^{-1} HCl and 1, 2 and 3 mol.L^{-1} H$_2$SO$_4$ at
233 RT for one week. Afterwards the samples were rinsed with deionized water, and SEM analysis and IEC
234 measurements were performed. Additionally, chlorine resistance of the membranes was tested in-situ
235 with solutions of 5 mol.L^{-1} NaCl at both anolyte and catholyte. A current density of 512 A m^{-2} was applied
236 and the potential was monitored over time. Periodically, a iR test was performed to determine the
237 membrane resistance. A change in resistance is due to damage of Cl$_2$ gas on the membrane. Fouling
238 resistance was tested with 1 mol.L^{-1} Ca(NO$_3$)$_2$ and 1 mol.L^{-1} K$_2$CO$_3$ solution at the anolyte and the
239 catholyte, respectively. A current density of 256 A m^{-2} was applied and the time until fouling (set at a
240 potential of 27 V) was reached was monitored. This fouling was a result of the formation of CaCO$_3$ at
241 the cathodic compartment due to the migration of Ca^{2+} through the CEM and the high pH at the catholyte.
242 Consecutively, the membranes were cleaned for 1h in 1 mol.L^{-1} H$_2$SO$_4$. The membrane resistance was
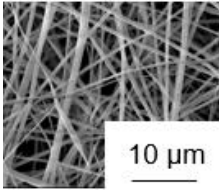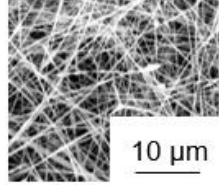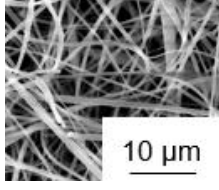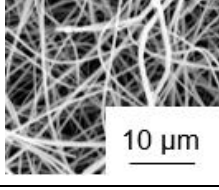243 measured before and after fouling and after cleaning.

3. RESULTS AND DISCUSSION

3.1 Production of the sulfonated silica-based nanofiber CEM

247 Inspired by the procedure for the direct electrospinning of pure silica nanofibers based on TEOS [44],
248 [45], the molar composition was adapted and extended to a TEOS/MPTES blend. As such, silica-based
249 nanofibers containing a MPTES functionality were produced via a reproducible and stable direct
250 electrospinning process for the first time. For optimal ionic properties, the amount of MPTES in the
251 nanofibers should be as high as possible. The sol production was optimized by varying the molar ratios
252 of the components used in a pure TEOS mixture (Table 1, Figure 1). At the initial molar ratios of 2:2:0.01
253 for ethanol:water:HCl, respectively (which are the optimal molar ratios for a pure TEOS sol-gel system),
254 a maximum TEOS/MPTES molar ratio of 1/0.1 could be obtained, resulting in successful electrospinning
255 of the sol into nanofibers. Afterwards, the nanofibers were oxidized in H$_2$O$_2$ to obtain the conversion of
256 -SH into -SO$_3$H. This resulted in an IEC of 0.7 mmol g^{-1}. Higher MPTES concentrations, without other
257 alterations of the sol composition, led to a film deposition instead of nanofibers during electrospinning.

258 This is due to a reduced reactivity of the sol by the presence of MPTES. This reduced reactivity results
259 in insufficient crosslinks in the network structure to allow nanofiber formation. Generally, the reaction
260 kinetics can be increased by changing the H_2O/TEOS (R) molar ratio. When R=2, as was the case,
261 incomplete hydrolysis occurs. This is desired in view of electrospinning to allow the formation of a stable,
262 electrospinnable sol [45]. However, with the presence of MPTES, R should be increased to improve the
263 reaction kinetics and network formation [51], [52]. As such, by increasing R to 3, a molar ratio of
264 TEOS/MPTES up to 1/0.4 could be reached. This resulted in a maximum IEC of 1.8 mmol g^{-1}. Higher
265 molar ratios of TEOS/MPTES were not possible to electrospin into nanofibers. However, although SEM
266 images show uniform nanofibers for the ratio of 1/0.4 (Table 1), this membrane showed little
267 macroscopic coherency due to insufficient interconnections again during the sol-gel synthesis, impeding
268 its use as a separation membrane. For electrochemical applications, it is important that the membrane
269 is robust, coherent and does not break during assembling and usage. It was observed that the
270 TEOS/MPTES 1/0.4 membrane did not allow this. Therefore the TEOS/MPTES molar ratio of 1/0.3 was
271 used as optimal membrane as this showed a much better mechanical coherence, and thus the resulting
272 IEC is 1.5 mmol g^{-1}. This is comparable to state-of-the-art polymeric cation-exchange nanofibers and
273 commonly used commercial membranes (e.g. the IEC of Nafion© and CMI-7000 is 0.9 and 1.6 mmol g^{-1},
274 respectively) [33], [53], [54].The nanofibers could be electrospun for several hours with a stable
275 process, resulting in a thick, coherent membrane (Supporting information Figure S1), optimal for
276 implementation in lab-scale EC setups, as shown in Figure 2. The membrane has a thickness of ±100
277 μm, consisting of many layers of fibers with a diameter of 352 ± 149 nm. After oxidation in H_2O_2, the
278 nanofiber structure is preserved with no significant change in fiber diameter (Figure 5).

279 Table 1: Sol-gel composition required for stable electrospinning of different TEOS/MPTES molar ratios, combined with the
280 corresponding IEC values after oxidation and SEM images of the membrane structure. The IEC increases upon increasing the
281 MPTES loading.

Molar ratios (-)					IEC (mmol g^{-1})	SEM image
TEOS	MPTES	EtOH	H_2O	HCl		
1	0.1	2	2	0.01	0.7 ± 0.1	
1	0.2	2	2.5	0.01	1.3 ± 0.0	
1	0.3	2	3	0.01	1.5 ± 0.0	
1	0.4	2	3	0.01	1.8 ± 0.0	

282

The successful bonding of the functional thiol groups in the silica-based nanofiber CEM was confirmed by ATR-FTIR spectroscopy (Figure 3). Signals corresponding to the silica network were observed and are indicated on Figure 3. Additionally, signals at 690 cm^{-1} were also observed, which are originating from Si-CH$_2$ vibration bonds [55]. Those Si-CH$_2$ bonds are only present in the MPTES group, thus proving the presence of the functional group in the silica-based network. As expected, the peak increases with increasing MPTES loading, which confirms the increasing IEC values after oxidation as discussed in Table 1.

290
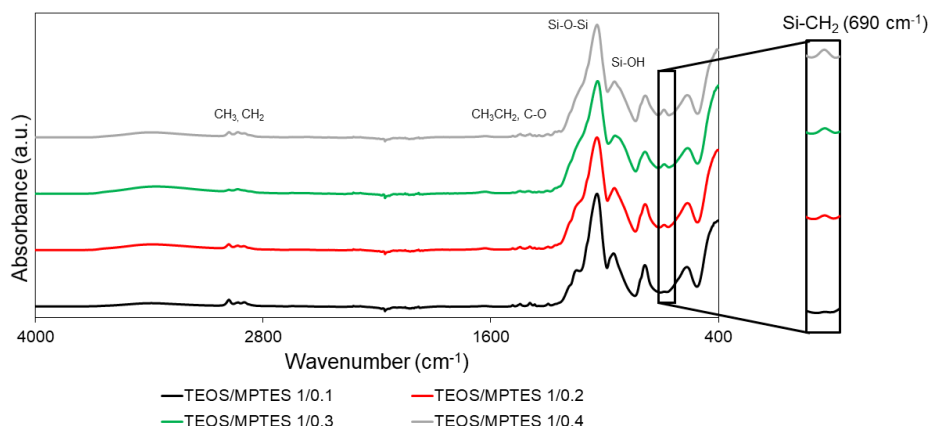
Figure 3: ATR-FTIR spectra of the silica-based nanofiber CEM with different MPTES loadings show an increased Si-CH$_2$ signal at 690 cm^{-1} with increasing amount of MPTES, proving the presence of the MPTES functional group on the nanofibers after electrospinning. All spectra are normalized based on the signal at 1076 cm^{-1} which is attributed to Si-O-Si vibrations.

Additionally, the successful oxidation of -SH into -SO$_3$H for TEOS/MPTES 1/0.3 was further characterized via XPS (Figure 4). Signals corresponding with O 1s (533 eV), C 1s (285 eV), Si 2s (155 eV) and Si 2p (104 eV) are observed, originating from the silica structure [56], [57]. Before oxidation, signals corresponding with sulphide (S^{2-}, 228.6 eV for S 2s and 163.8 eV for S 2p) and sulphite (SO$_3^{2-}$, 232.3-233 eV for S 2s and 168.2-168.4 eV for S 2p) are present with around 60-70% corresponding to sulphide [47], [49], [58], [59]. After oxidation in H$_2$O$_2$ for 24h at RT, all signals corresponding with sulphide disappeared and only signals corresponding with sulphite remain. These results confirm the successful oxidation of -SH into -SO$_3$H, leading to the IEC values as mentioned in Table 1.
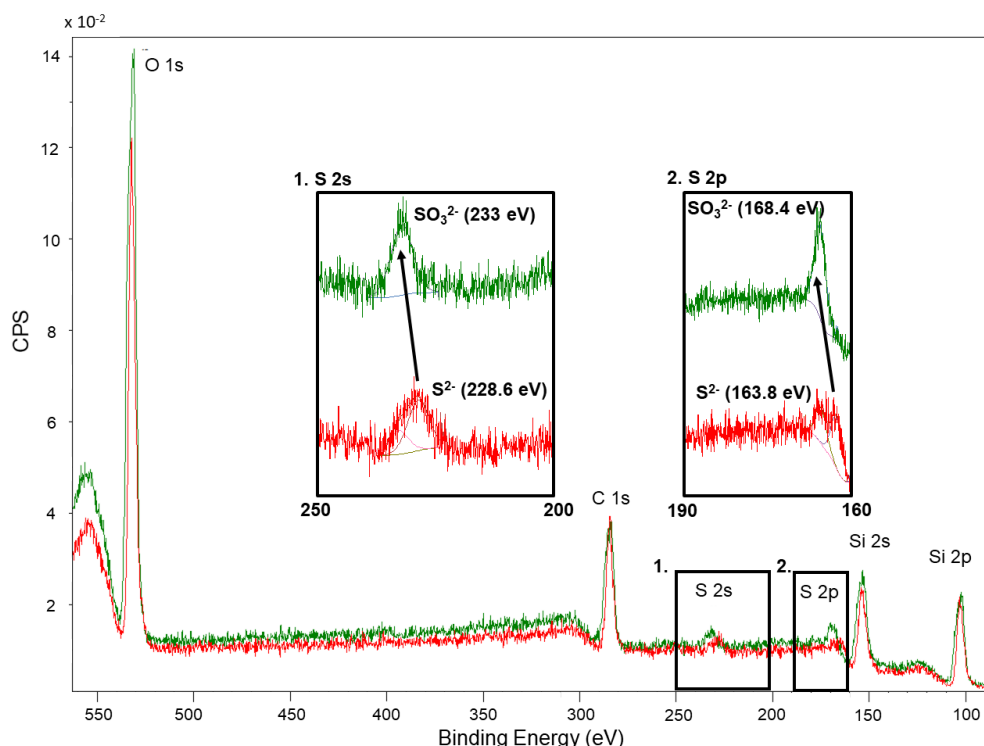
302

Figure 4: XPS analysis of the nanofiber CEM before oxidation (red line) and after oxidation (green line). The shifts in signals indicate the successful oxidation of the membrane.

The developed silica-based nanofiber CEM showed excellent ionic properties (see IEC values in Table 1). However, due to the presence of the highly hydrophilic -SO_3H groups and the porous structure of the nanofiber membrane, the membrane showed no water-barrier properties. Therefore further functionalization to ensure the anolyte-catholyte compartment separation was necessary.

3.2 Design of the optimal sulfonated silica-based nanofiber CEM suitable for electrochemical processes

For implementation in electrochemical systems, the CEM must act as a mechanically robust separation barrier with no water cross-over. In this research, the separation performance was obtained via a novel, alternative method which allows for the nanofiber morphology to be preserved. Instead of processing the nanofibers into a dense membrane via a pore-filling matrix, the nanofibers were functionalized with hydrophobic groups. As a result, the membrane has water-repellent properties and acts as a separation unit, despite the porous structure. In this way, the excellent ionic properties of the nanofibers could be preserved while allowing separation of the compartments. Generally, silica-based materials are known for their ease of functionalization with chlorosilanes [60], [61]. Due to incomplete hydrolysis and condensation during the sol-gel synthesis (as a result of limiting the amount of H_2O during synthesis), many silanol groups remain present on the structure. These silanol groups react with chlorosilanes to form a stable silica structure with Si-R bonds, as shown in Figure 5. Different chlorosilanes with varying alkyl chains (Cl-TMS, Cl-TES, Cl-TBS, Cl-THS, Cl-BdMS, Cl-HdMS, Cl-OdMS) were used as functionality and their hydrophobicity was measured using WCA measurements (Figure 5,Table 2). A hydrophobic membrane could be produced by using long alkyl chlorosilanes such as Cl-THS and Cl-OdMS, which showed excellent water barrier properties. WCAs were measured both before and after immersion in 1 mol.L^{-1} NaCl, to ensure the water-repellent behaviour independently of the ionic group present on the membrane.

9

Procedure
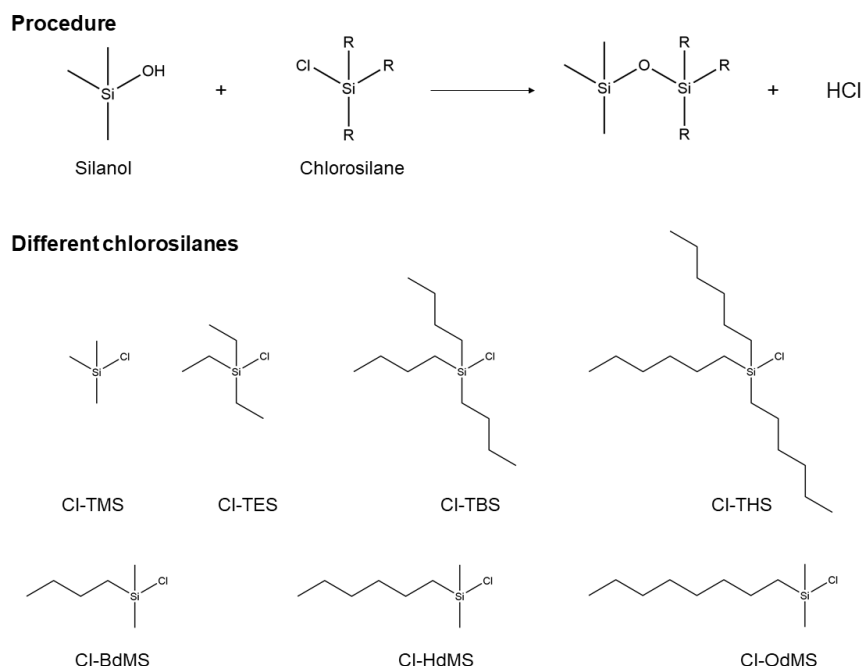

Silanol + Chlorosilane → (product) + HCl

Different chlorosilanes

Cl-TMS   Cl-TES   Cl-TBS   Cl-THS

Cl-BdMS   Cl-HdMS   Cl-OdMS

327
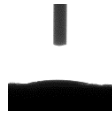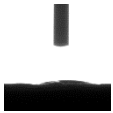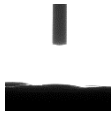
328 Figure 5: Functionalization of a silica network with chlorosilanes: procedure and different chlorosilanes used in this research. Cl-
329 TMS = chloro-trimethylsilane, Cl-TES = chloro-triethylsilane, Cl-TBS = chloro-tributylsilane, Cl-THS = chloro-trihexylsilane, Cl-
330 BdMS = chloro-butyldimethylsilane, Cl-HdMS = chloro-hexyldimethylsilane, Cl-OdMS = chloro-octyldimethylsilane.

331 Despite the presence of the water-repellent alkyl groups, the membranes still showcased excellent
332 affinity towards ions, as proven by the IEC values in Table 2. Both Cl-THS and Cl-OdMS showed a high
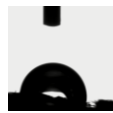333 WCA both before and after immersion in 1 mol.L^{-1} NaCl. However, for Cl-THS the WCA decreased
334 substantially after immersion in NaCl and some hydrophilic spots were observed, indicating that the
335 functional group is not completely effective as hydrophobic component. For Cl-OdMS, the hydrophobic
336 shielding was better and therefore, the functionalization with Cl-OdMS resulted in the most desired
337 properties and further tests were all performed on this membrane. Figure 6 shows SEM images after
338 each step of the production process towards the optimized nanofiber CEM. It is visible that both oxidation
339 in H_2O_2 and functionalization in Cl-OdMS do not influence the morphology of the membrane structure.
340 However, a clear porous fiber structure remains visible, with a significant increase in fiber diameter after
341 immersion in Cl-OdMS. This can be a result of the long alkyl chains forming a film around the individual
342 nanofibers during functionalization, and thus increasing the fiber diameter. Using the fiber diameter and
343 the theoretical calculations from Eq. (1) and Eichhorn et al. [50], the porosity, pore size diameter an
344 specific surface area of the nanofiber membrane can be calculated as 0.89, 19 µm and 8 m² g^{-1},
345 respectively. In Table 3, a comparison is given with other fibrous and non-fibrous porous CEMs
346 described in literature. The silica-based CEM from this research has a relatively large porosity and pore
347 size diameter due to the nanofiber structure. Due to this high pore size, a relatively high water uptake is
348 also observed (108 ± 15 %), despite the hydrophobic nature. It should be noted that properties such as
349 porosity and pore size diameter are often measured or calculated differently and, as such, should be
350 compared carefully.

351 It is observed that the IEC slightly decreased from 1.5 to 1.3 mmol g^{-1}, due to the hydrophobic treatment.
352 This could be attributed to the additional chemical groups originating from the Cl-OdMS that contribute
353 to the total weight of the membranes, or a slight steric hindrance of the ionic groups. To investigate this,
354 the mass difference of the oxidized nanofiber membrane before and after functionalization with Cl-OdMS
355 was measured using TGA (Supporting information Figure S2). Still, no significant mass difference was
356 observed after functionalization in Cl-OdMS (when accounting for the evaporation of solvents).
357 Consequently, the decrease in IEC is not a result of the additional weight of Cl-OdMS but is most likely
358 attributed to the steric hindrance. The presence of long alkyl chains can block the ionic groups, limiting
359 their accessibility for ion-exchange and thus lowering the IEC. However, since the reduction in IEC is
360 limited, the effect of steric hindrance is expected to be small. In addition, the thermal resistance was

determined via TGA as well. For some electrochemical applications, an increased temperature (ranging from 100 to > 200°C) can improve the efficiency of the process [62]–[65]. Around 100°C a small drop is observed in the TGA analysis, which is attributed to the loss of absorbed solvents such as water [66]. Around 400°C, another significant drop is observed, indicating the degradation of the organic components (Supporting information Figure S2). As a result, the nanofiber CEM shows an excellent thermal resistance up to 400°C, which is already beneficial for many applications. At higher temperatures, only the inorganic backbone remains.

Table 2: IEC and WCA values before and after immersion in 1 mol.L^{-1} NaCl for the nanofiber CEM functionalized with different alkyl chlorosilanes. The results show the excellent ion transport combined with water barrier properties for the nanofiber CEM functionalized with Cl-OdMS.

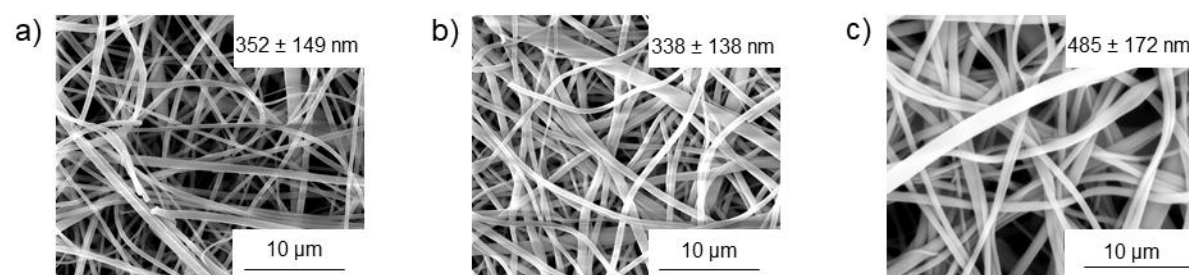|	Cl-TMS	Cl-TES	Cl-TBS	Cl-THS	Cl-BdMS	Cl-HdMS	Cl-OdMS
IEC (mmol g^{-1})	1.4 ± 0.0	1.4 ± 0.0	1.3 ± 0.0	1.3 ± 0.0	1.3 ± 0.0	1.2 ± 0.1	1.3 ± 0.0
WCA (°)	0 ± 0	0 ± 0	107 ± 10	119 ± 8	0 ± 0	0 ± 0	124 ± 10
WCA after 24h in 1 mol.L^{-1} NaCl (°)	0 ± 0	0 ± 0	0 ± 0	84 ± 29	0 ± 0	0 ± 0	122 ± 5

Figure 6: SEM-images a) directly after electrospinning, b) after oxidation in H$_2$O$_2$ and c) after functionalization in Cl-OdMS.

Table 3: Overview of properties for different fibrous and non-fibrous porous CEMs as described in literature and in this work. Porosity and pore size diameter are often measured in different ways and are therefore difficult to compare.

Material	Method	Porosity (-)	Pore size diameter (μm)	IEC (mmol g^{-1})	WU (%)	REF
sPPO nanocomposite	Phase inversion	0.35-0.62	-	1.0-1.4	29-58	[67]
sPES	Phase inversion	-	0.05-0.20	0.7	239-275	[68]
PVC	Phase inversion	0.24-0.43	-	1.3-2.8	30-41	[69]
PAN	Electrospinning	0.84	-	0.5-0.6	-	[70]
PS	Electrospraying	0.75	1.87	1.3	-	[71]
Silica	Electrospinning	0.89	19	1.3	108	This work

The mechanical robustness of the membranes is a crucial parameter in the overall performance of the membrane in electrochemical systems. Tensile tests were performed on the nanofiber CEM at dry and

11

379 wet conditions (Figure 7). Despite forming a coherent membrane after electrospinning, its general tensile
380 strength is rather low. To improve the robustness of the nanofiber CEM, the membrane was sandwiched
381 in between two reinforcing layers made of low-density glass fiber woven fabric (see Figure 1). These
382 support layers do not influence the ionic and separation properties of the nanofiber CEM because of
383 their high porosity. While the UTS and Young's modulus of the nanofiber membrane in dry conditions
384 are 4.6 ± 0.7 MPa and 439 ± 36 MPa, respectively, the UTS and Young's modulus with reinforcing layers
385 are 21.5 ± 3.3 MPa and 1916 ± 143 MPa, respectively. This is an increase of 367% in strength and
386 336% in Young's modulus, proving the positive effect of the supporting layers on the mechanical
387 robustness (Figure 7 and Supporting information Table S1). Note that the tensile tests of the reinforced
388 membrane were performed until the point of failure of the nanofiber CEM (1.2% strain for the dry state
389 and 3.2% for the wet state) and the UTS was determined as the maximum value within that region. Due
390 to the excellent mechanical properties of the reinforced membrane, this structure was used in all further
391 testing. Based on the results in this section, an optimal sulfonated silica-based nanofiber CEM was
392 obtained, which could be subjected to lab-scale tests to assess its electrochemical performance, as
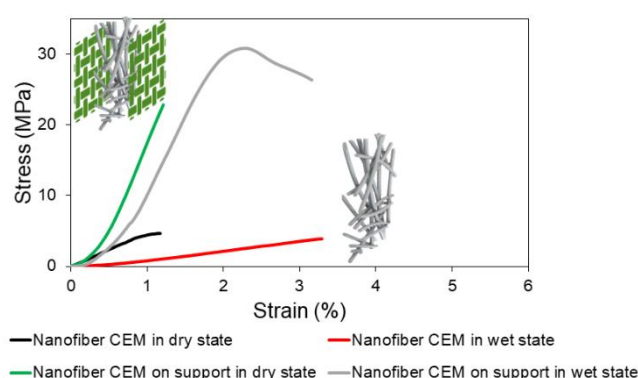393 detailed in Section 3.3.

394

395 Figure 7: Example of stress-strain curves of the nanofiber CEM show the increased failure strain for the wet sample and the
396 improved strength in the presence of the supporting layers. The tensile test with supporting layers was performed until the
397 nanofiber membrane reached its failure strain at 1.2% (dry) or 3.2% (wet). The UTS was, as such, determined as the maximum
398 value within that region.

399 *3.3 General lab-scale performance of the optimized sulfonated silica-based nanofiber CEM*

400 The newly developed hydrophobic sulfonated silica-based nanofiber CEM, sandwiched between
401 reinforcing layers, could be implemented in a lab-scale EC to act as selective separation membrane
402 between the anolyte and catholyte compartment in water treatment processes. To assess the
403 performance of the nanofiber membrane, a comparison was made with the commercially available CEM:
404 CMI-7000 (from Membrane International). This sulfonated polystyrene-based CEM is commonly used
405 in many water treatment applications due to its robustness [11], [72], [73]. The performance of this
406 commercial membrane was set as target for the desired performance of the nanofiber CEM. The
407 performance was evaluated based on membrane resistance, Coulombic efficiency, permselectivity,
408 energy demand, water flux, ion selectivity, acidic resistance, chlorine resistance and fouling resistance.

409 The membrane resistance was measured after initial usage ($R_{initial}$) and after 24h of usage (R_{24h}). The
410 initial resistance of the newly developed nanofiber CEM is higher than for the commercial CMI-7000
411 (Table 4). However, after 24h the resistance of the nanofiber CEM has become significantly lower. This
412 evolution in resistance is attributed to the gradual acclimatization of the membrane. Before testing, all
413 membranes receive a pre-treatment which consists of 24h submersion in a salt solution that contains
414 the same cations as the intended test solution. This is done to assure the best performance. However,
415 in contrary to the CMI-7000 reference, the nanofiber CEM has a high hydrophobicity (WCA of 67 ± 8°
416 for CMI-7000 vs. 124 ± 10° for the nanofiber CEM), resulting in a low affinity for water compounds
417 initially. Therefore, the pre-treatment is most likely not completed after 24h for the nanofiber CEM and
418 a higher membrane resistance is observed. During testing, the resistance decreases gradually due to
419 additional contact with the salt solution, resulting in a superior performance compared to the CMI-7000
420 reference after pre-treatment. Note that the newly developed nanofiber CEM shows a lower resistance
421 than CMI-7000 despite its lower IEC (1.3 vs. 1.6 mmol g^{-1}). This is attributed to the interesting

morphology of the nanofiber membrane for ion transport, namely the presence of ion-transport channels along the fiber length and a high specific surface area of the nanostructure with many accessible ionic groups, resulting in improved ion transport despite the lower IEC [34], [35]. Due to the elimination of a pore-filling matrix in this research, the nanofiber's morphology effect on the membrane's performance can be fully exploited.

The Coulombic efficiency was calculated based on the ion migration through the membranes after 48h. The results show a similar efficiency and performance for both membranes, proving an already effective performance of the newly developed silica-based nanofiber CEM (Table 4). The selectivity number was calculated to be 0.90 ± 0.00 for the nanofiber CEM and 0.88 ± 0.00 for CMI-7000, proving a similar permselectivity for both membranes. For prolonged use, the energy demand is similar at a current density of 128 A m^{-2} and the energy demand is slightly higher for the nanofiber CEM at 256 A m^{-2}. These results are also comparable to values found in literature [74], [75]. Additionally, the water flux through the membranes was investigated and it was observed that the nanofiber CEM had a water flux of 3.2 ± 1.6 mol H_2O/mol Na^+, whereas the CMI-7000 reference had a water flux of 5.7 ± 1.6 mol H_2O/mol Na^+. Despite the porous membrane structure of the nanofiber CEM, the water cross flow is lower, most likely because of its hydrophobicity due to the functionalization with Cl-OdMS. It is known in literature that electrospun nanofibers have a high surface roughness, therefore entrapping air and increasing the hydrophobicity compared to their corresponding film materials [76], [77]. However, in the electrochemical cell, the air entrapment will eventually disappear and the hydrophobicity will be completely due to nature of the hydrophobic groups. When a significant concentration difference is present, the osmotic flow through the nanofiber CEM tends to be higher (16% vs. 5.6 %).

The ion selectivity test shows an ion migration preference of $K^+ > Na^+ > Li^+$. In Table 4 the relative amount of Li^+, Na^+ and K^+ in the anolyte is given after 48h compared to 0h, with lower amounts resulting from cations that have migrated through the membrane. This ionic preference is also commonly found for other CEMs and is strongly influenced by the hydration shells of the cations. Ions with a larger hydration shell will migrate slower than ions with a smaller hydration shell. This hydration shell is influenced by both the charge and atomic radius of the cations, resulting in a larger hydration shell for smaller cations and cations with a higher charge (thus the hydration shell increases from $K^+ < Na^+ < Li^+$). Cations with a smaller hydration shell also have a lower dehydration energy, this is the energy required to break down the hydration shell. During electrolysis, the hydration shell gets partially disrupted when ions migrate through the membrane. Ions with a smaller hydration shell, and thus smaller dehydration energy, will therefore migrate more easily through the membrane [78]–[83]. Additionally, under a high applied voltage, the K+/Na +/Li+ selectivity gradually converges to their mobility ratio. This mobility difference can be attributed to the contrasting exchange rates of the ion's hydration water. The exchange rate discrepancy implies that the hydrated Li+ is more rigid than K+, resulting in a larger drifting resistance in water and a lower ion mobility [84], [85]. The general trends observed for both the nanofiber CEM and CMI-7000 confirm this behaviour and are in line with what is expected. So a strong selectivity can be observed for the nanofiber CEM despite its higher porosity, similar as for the dense CMI-7000.

In general, the newly developed silica-based nanofiber CEM shows excellent performances in lab-scale ECs, with results already in line with commercially available membranes (Table 4). Furthermore, the nanofiber CEM's straightforward and cheap production method shows a high potential for future industrial applications.

Table 4: Membrane resistance after 0 and 24 h of usage, Coulombic efficiency based on ion migration, energy consumption and ion selectivity after 48h of both the nanofiber CEM and commercial CMI-7000 reference.
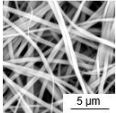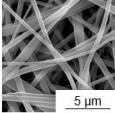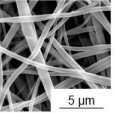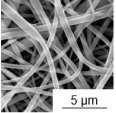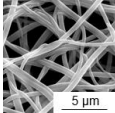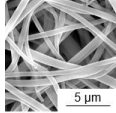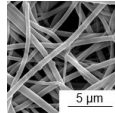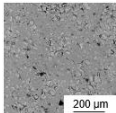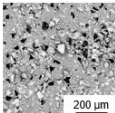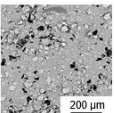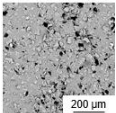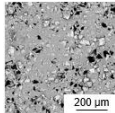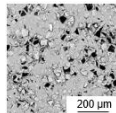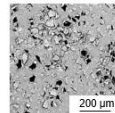
	$R_{initial}$ (*10^{-3} Ω m²)	R_{24h} (*10^{-3} Ω m²)	CE (%)		E_c (Wh g^{-1})		C/C$_0$ after 48h (%)		
			128 A m^{-2}	256 A m^{-2}	128 A m^{-2}	256 A m^{-2}	Li	Na	K
Nanofiber CEM	4.9 ± 1.1	3.2 ± 0.4	69 ± 3	71 ± 2	6.1 ± 0.7	7.5 ± 0.5	98 ± 1	87 ± 5	79 ± 8

CMI-7000 (Reference)	4.6 ± 0.0	4.6 ± 0.0	75 ± 11	73 ± 6	6.4 ± 1.5	6.9 ± 0.7	87 ± 1	80 ± 2	69 ± 2

3.4 Chemical resistance of the optimized sulfonated silica-based nanofiber CEM

For many electrochemical processes, the chemical and chlorine resistance of the IEM is crucial for the large-scale electrochemical application. The newly developed sulfonated silica-based nanofiber CEM has an excellent chemical stability in the pH range 0-10, similar to the CMI-7000 reference (pH 1-10). At alkaline conditions (pH >10), the Si-O-Si bonds within the nanofibers debond resulting in membrane degradation [86]. Additionally, the chemical resistance in two commonly used acidic solutions, namely HCl and H_2SO_4, was tested at various concentrations via immersion (Table 5). The nanofiber membranes showed extraordinary resistance without fiber damage. In these extreme conditions, the IEC values are slightly lower (from 1.3 to 1 mmol g^{-1}), which is most likely attributed to a small loss in ionic groups over time, which is generally known as ageing, and could be a consequence of the absence of pre-treatment of the membranes for this specific test [87], [88]. For the CMI-7000 reference, the IEC remained more or less the same, but microscopic holes were visible on the SEM images, which can be attributed to the top-layer that starts to comes loose in these conditions. However, this was not yet noticeable on a macroscopic scale.

Table 5: IEC values and SEM images of the nanofiber CEM and CMI-7000 reference after immersion in HCl and H_2SO_4 for one week show an overall good chemical stability of the membranes.

		REF	1M HCl	2M HCl	3M HCl	1M H_2SO_4	2M H_2SO_4	3M H_2SO_4
Nanofiber CEM	IEC (mmol g^{-1})	1.3 ± 0.0	1.0 ± 0.0	1.0 ± 0.1	1.0 ± 0.0	1.0 ± 0.0	1.0 ± 0.0	0.9 ± 0.2
	SEM image							
CMI-7000 (Reference)	IEC (mmol g^{-1})	1.6 ± 0.1	1.4 ± 0.0	1.5 ± 0.0	1.5 ± 0.0	1.5 ± 0.0	1.6 ± 0.0	1.6 ± 0.0
	SEM image							

The chlorine stability of the membranes was tested in an EC in which chlorine gas was produced as a result of the anodic reactions taking place (Eq. 4).

$$2Cl^- \text{ (aq)} \rightarrow Cl_2 \text{ (g)} + 2e^- \tag{4}$$

Figure 8a shows that there is no significant change in resistance due to the presence of chlorine. So there is no degradation of ionic groups, both for the newly developed nanofiber CEM and the CMI-7000 reference. The initial decrease in resistance for the nanofiber CEM is attributed to the earlier discussed pre-treatment. SEM images show no significant damage of the membrane structures on a microscopic scale (Figure 8b and 8c), which was confirmed by ATR-FTIR spectroscopy as well for the nanofiber CEM (see Supporting information Figure S3). On a macroscopic scale, the CMI-7000 reference started to show some discolouring, most likely attributed to some initial degradation. The nanofiber CEM remained completely identical as before the test (Supporting information Figure S4). Therefore it is

concluded that the nanofiber CEM has an excellent chlorine resistance, and generally chemical resistance, slightly exceeding that of the commercially available membrane.
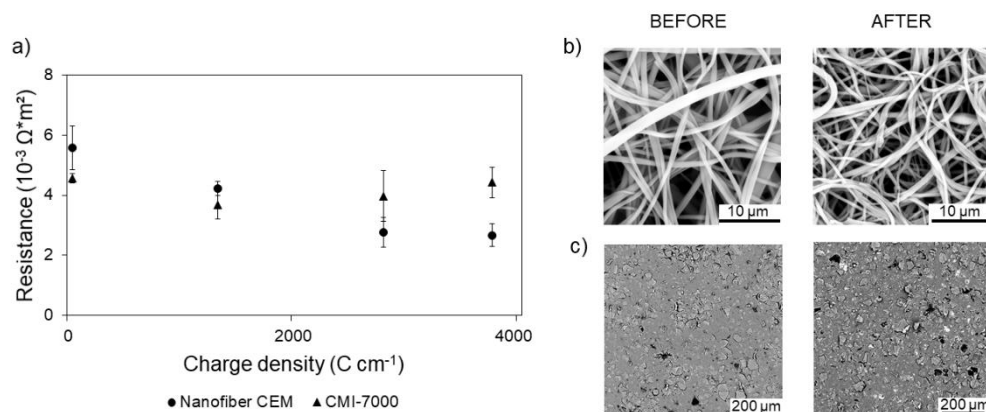

Figure 8: a) Membrane resistance over time during chlorine production of the EC. The nanofiber CEM shows an excellent resistance against chlorine gas, comparable to the commercially CMI-7000. b) SEM images of the nanofiber CEM before and after exposure to chlorine, c) SEM images of CMI-7000 before and after exposure to chlorine.

3.5 Fouling performance of the optimized sulfonated silica-based nanofiber CEM

A very important phenomenon of ion-exchange membranes for water treatment applications is fouling, and more specifically scaling, upon long-term usage [89], [90]. Scaling products consist mainly of Ca^{2+} and/or Mg^{2+} and need to be removed. This is done by harsh acidic cleaning to dissolve the precipitates, often damaging the membrane and limiting their industrial applicability. Alternatively, the precipitations can also be removed by a process called polarity reversal in which the current is reversed for a short period. However, this method requires the need for expensive, corrosion resistant electrodes such as platinum instead of stainless steel [15], [16]. The fouling resistance of the nanofiber CEM was tested in a lab-scale EC in which $CaCO_3$ fouling precipitates were formed on the membrane at the cathodic compartment (pH > 5). Figure 9 shows the evolution of the membrane resistance before and after fouling, and after a cleaning action with a 1 mol.L^{-1} H_2SO_4 solution, for both the nanofiber CEM and CMI-7000 during three cycles. The nanofiber CEM does not show an increased resistance after fouling (Figure 9a). This means that the fouling products only occur on the surface of the membrane and are easily removed, even without needing an acid. On the contrary, CMI-7000 shows a clear resistance increase after fouling and needs a cleaning action to remove the fouling products (Figure 9b). Both membranes show constant behaviour over multiple cycles. Note that the slight decrease in resistance observed for the nanofiber CEM is attributed to the pre-treatment, as discussed in Section 3.3. It can be concluded that the nanofiber CEM shows promising self-cleaning properties. This is an important and innovative CEM property demonstrating the potential of the newly developed sulfonated silica-based nanofiber CEM in industrial applications.
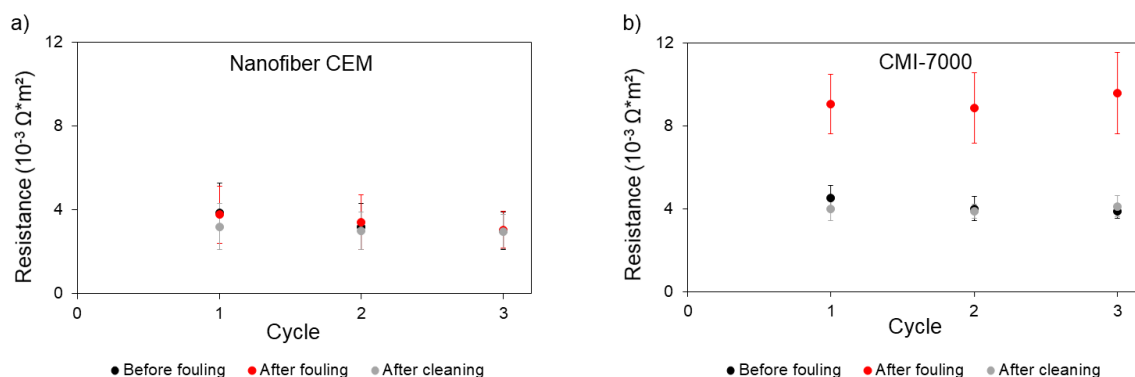

Figure 9: Membrane resistance before and after fouling and after 1 h of cleaning with 1M H_2SO_4 over 3 cycles for a) the nanofiber CEM and b) CMI-7000. The nanofiber CEM showed no increase in resistance after fouling, indicating that the fouling products are easily removed and are mostly found on the exterior surface of the membrane.

15

526 SEM images after the fouling and cleaning cycles show no degradation of the nanofiber membrane and
527 small microscopic holes for CMI-7000 as a result of the cleaning action in 1 mol.L^{-1} H$_2$SO$_4$ (Figure 10).
528 ATR-FTIR spectra (Supporting information Figure S5) confirmed no structural degradation of the
529 nanofiber CEM. Additionally, no trace amounts of CaCO$_3$ were detected on the membranes after
530 cleaning. To confirm the self-cleaning ability of the nanofiber CEM, SEM images were also taken in the
531 case of no cleaning action (Figure 10). For CMI-7000, there is a complete coverage of the membrane
532 surface of CaCO$_3$ precipitation, as expected from the resistance data. For the nanofiber CEM, only small
533 CaCO$_3$ precipitates are visible and the nanofibers are still clearly visible and accessible for ion transport,
534 proving that most of the precipitates were removed. A possible explanation for the self-cleaning ability
535 of the nanofiber CEM can be found in the high hydrophobicity of the membrane, which is typical for
536 silica-based nanofibers produced via the direct electrospinning of a sol, as described in Section 3.1.
537 Surfaces with a high contact angle have a low surface energy, which is accompanied with low adhesion
538 forces for scaling/fouling products [91].
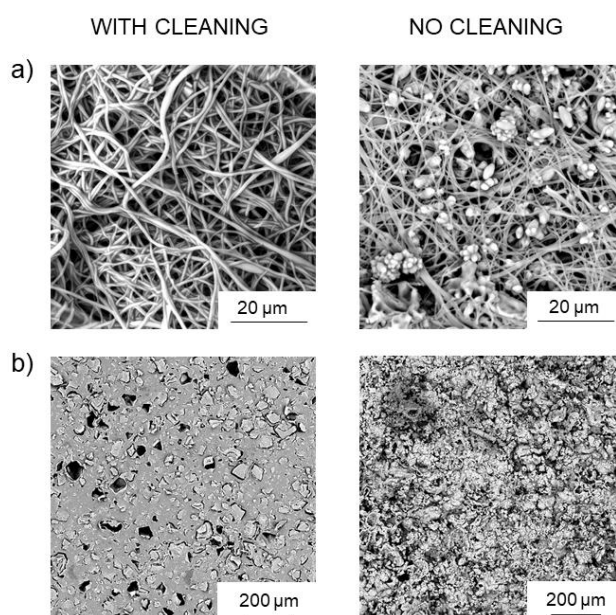
540 Figure 10: SEM-images of a) nanofiber CEM and b) CMI-7000 after fouling in the case of a cleaning action and no cleaning action.
541 Both membranes show no degradation due to fouling and/or cleaning. However, CMI-7000 is completely covered with CaCO$_3$
542 when no cleaning is done, whereas the nanofiber CEM shows only small spots where CaCO$_3$ precipitates remains present due to
543 its self-cleaning ability.

544 To further prove their potential, fouling tests were performed for two different cases: a) with a cleaning
545 action in H$_2$SO$_4$ after each cycle and b) with no cleaning step at all (Figure 11). For each case, the time
546 until fouling was monitored over 3 cycles at 256 A m^{-2}.
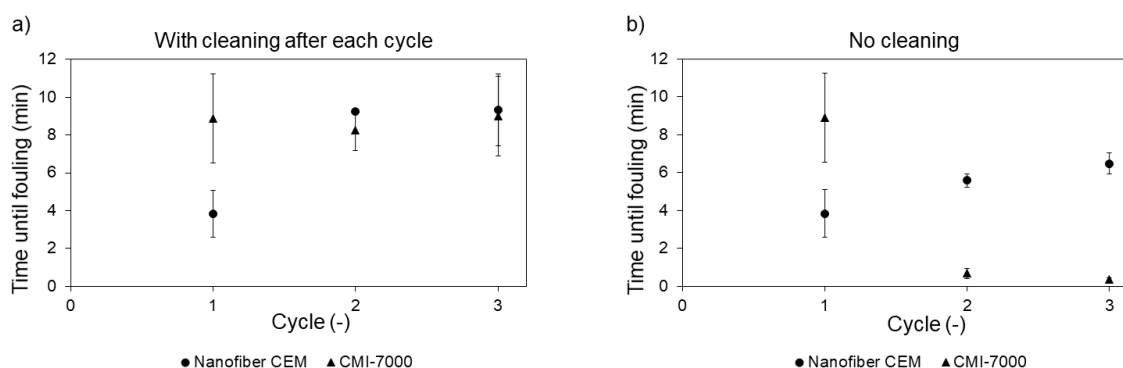
548 Figure 11: Time until fouling occurred (determined by the potential that reached 27 V) for the membranes with a) a cleaning action
549 in H$_2$SO$_4$ after each cycle and b) no cleaning. The nanofiber CEM shows self-cleaning properties with no drop in time over multiple
550 cycles.

551 For the silica-based nanofiber CEM, it was observed that fouling occurs more quickly than for CMI-7000
552 during the first cycle, but tends to go slower during the next cycles after cleaning in H_2SO_4, reaching the
553 same range as CMI-7000 (Figure 11a). This low time for the nanofiber CEM during cycle 1 could again
554 be a consequence of the earlier discussed pre-treatment. When the cleaning action in H_2SO_4 is omitted,
555 the time until fouling for CMI-7000 drops almost to zero, while the nanofiber CEM shows a similar trend
556 as in the case of cleaning in H_2SO_4, however, with a slower increase. These results prove the
557 requirement of a cleaning action for the commercial CMI-7000, whereas for the nanofiber CEM this can
558 be eliminated due to its self-cleaning ability.

559 4   CONCLUSION

560 A sulfonated silica-based nanofiber CEM with superior self-cleaning ability during fouling was produced.
561 The nanofibers were produced for the first time via direct electrospinning of a sol-gel solution, consisting
562 of the co-condensation of TEOS and MPTES. Post-functionalization with hydrophobic alkyl
563 chlorosilanes enables to produce membranes with excellent water barrier properties without the need
564 of an additional pore-filling matrix, resulting in an innovative nanofiber CEM. The produced CEM, with
565 an IEC of 1.3 mmol g^{-1}, showcased a resistance of 3.2 ± 0.4 Ω m², which is lower than the commonly
566 used commercially available CEM CMI-7000. Lab-scale performance tests showed an excellent
567 behaviour of the nanofiber CEM in view of water treatment applications. Furthermore, the nanofiber
568 CEM has an outstanding chemical resistance, in acidic solutions and for chlorine gas, which is of utmost
569 importance for water treatment applications. These properties, combined with the self-cleaning ability of
570 the nanofiber CEM during fouling, prove that the membrane has beneficial properties and a high
571 potential for industrial water treatment applications.

572

578

579 CONFLICT OF INTEREST

580 The authors declare no conflict of interest.

581   [1]   J. Radjenovic and D. L. Sedlak, "Challenges and Opportunities for Electrochemical Processes
582   as Next-Generation Technologies for the Treatment of Contaminated Water," *Environ. Sci.*
583   *Technol.*, vol. 49, no. 19, pp. 11292–11302, 2015, doi: 10.1021/acs.est.5b02414.

584   [2]   B. P. Chaplin, "Critical review of electrochemical advanced oxidation processes for water
585   treatment applications," *Environ. Sci. Process. Impacts*, vol. 16, no. 6, pp. 1182–1203, 2014,
586   doi: 10.1039/c3em00679d.

587   [3]   O. J. Murphy, G. Duncan Hitchens, L. Kaba, and C. E. Verostko, "Direct electrochemical
588   oxidation of organics for wastewater treatment," *Water Res.*, vol. 26, no. 4, pp. 443–451, 1992,
589   doi: 10.1016/0043-1354(92)90044-5.

590   [4]   F. C. Moreira, R. A. R. Boaventura, E. Brillas, and V. J. P. Vilar, "Electrochemical advanced
591   oxidation processes: A review on their application to synthetic and real wastewaters," *Appl.*
592   *Catal. B Environ.*, vol. 202, pp. 217–261, 2017, doi: 10.1016/j.apcatb.2016.08.037.

593   [5]   Y. Feng, L. Yang, J. Liu, and B. E. Logan, "Electrochemical technologies for wastewater
594   treatment and resource reclamation," *Environ. Sci. Water Res. Technol.*, vol. 2, no. 5, pp. 800–
595   831, 2016, doi: 10.1039/c5ew00289c.

596   [6]   R. Gao, S. Mosquera-Romero, E. Ntagia, X. Wang, K. Rabaey, and L. Bonin, "Electrochemical
597   Separation of Organic and Inorganic Contaminants in Wastewater," *J. Electrochem. Soc.*, vol.
598   169, no. 3, 2022.

599   [7]   H. Strathmann, "Ion-Exchange Membranes," 1992.

600   [8]   T. Xu, "Ion exchange membranes : State of their development and perspective," vol. 263, no. 2,
601   pp. 1–29, 2005, doi: 10.1016/j.memsci.2005.05.002.

602   [9]   J. Ran *et al.*, "Ion exchange membranes: New developments and applications," *J. Memb. Sci.*,
603   vol. 522, pp. 267–291, 2017, doi: 10.1016/j.memsci.2016.09.033.

604   [10] R. K. Nagarale, G. S. Gohil, and V. K. Shahi, "Recent developments on ion-exchange
605   membranes and electro-membrane processes," vol. 119, pp. 97–130, 2006, doi:
606   10.1016/j.cis.2005.09.005.

607   [11] G. V. Talekar, P. Sharma, A. Yadav, P. Clauwaert, K. Rabaey, and S. Mutnuri, "Sanitation of
608   blackwater via sequential wetland and electrochemical treatment," *npj Clean Water*, vol. 1, no.
609   1, pp. 1–9, 2018, doi: 10.1038/s41545-018-0014-x.

610   [12] G. V. Talekar and S. Mutnuri, "Membrane Selection for Electrochemical Treatment of Septage,"
611   *Front. Energy Res.*, vol. 8, no. February, pp. 1–12, 2020, doi: 10.3389/fenrg.2020.00020.

612   [13] Y. Yang, L. Lin, L. K. Tse, H. Dong, S. Yu, and M. R. Hoffmann, "Membrane-separated
613   electrochemical latrine wastewater treatment," *Environ. Sci. Water Res. Technol.*, vol. 5, no. 1,
614   pp. 51–59, 2019, doi: 10.1039/c8ew00698a.

615   [14] Y. Yang, L. Lin, L. K. Tse, H. Dong, S. Yu, and M. R. Hoffmann, "Membrane-separated
616   electrochemical latrine wastewater treatment," *Environ. Sci. Water Res. Technol.*, vol. 5, no. 1,
617   pp. 51–59, 2019, doi: 10.1039/c8ew00698a.

618   [15] M. A. C. K. Hansima *et al.*, "Fouling of ion exchange membranes used in the electrodialysis
619   reversal advanced water treatment: A review," *Chemosphere*, vol. 263, p. 127951, 2021, doi:
620   10.1016/j.chemosphere.2020.127951.

621   [16] S. Suwal, J. Amiot, L. Beaulieu, and L. Bazinet, "Effect of pulsed electric field and polarity
622   reversal on peptide/amino acid migration, selectivity and fouling mitigation," *J. Memb. Sci.*, vol.
623   510, pp. 405–416, 2016, doi: 10.1016/j.memsci.2016.03.010.

624   [17] W. Garcia-Vasquez, L. Dammak, C. Larchet, V. Nikonenko, and D. Grande, "Effects of acid-
625   base cleaning procedure on structure and properties of anion-exchange membranes used in
626   electrodialysis," *J. Memb. Sci.*, vol. 507, pp. 12–23, 2016, doi: 10.1016/j.memsci.2016.02.006.

627   [18] I. Atamanenko, A. Kryvoruchko, and L. Yurlova, "Study of the scaling process on membranes,"
628   *Desalination*, vol. 167, no. 1–3, pp. 327–334, 2004, doi: 10.1016/j.desal.2004.06.142.

629　[19]　M. Asraf-Snir, J. Gilron, and Y. Oren, "Gypsum scaling of anion exchange membranes in
630　　　　electrodialysis," *J. Memb. Sci.*, vol. 520, pp. 176–186, 2016, doi:
631　　　　10.1016/j.memsci.2016.07.013.

632　[20]　J. Kim and T. I. Yoon, "Direct observations of membrane scale in membrane bioreactor for
633　　　　wastewater treatment application," *Water Sci. Technol.*, vol. 61, no. 9, pp. 2267–2272, 2010,
634　　　　doi: 10.2166/wst.2010.124.

635　[21]　H. Guo, F. You, S. Yu, L. Li, and D. Zhao, "Mechanisms of chemical cleaning of ion exchange
636　　　　membranes: A case study of plant-scale electrodialysis for oily wastewater treatment," *J.*
637　　　　*Memb. Sci.*, vol. 496, pp. 310–317, 2015, doi: 10.1016/j.memsci.2015.09.005.

638　[22]　Q. Wang, P. Yang, and W. Cong, "Cation-exchange membrane fouling and cleaning in bipolar
639　　　　membrane electrodialysis of industrial glutamate production wastewater," *Sep. Purif. Technol.*,
640　　　　vol. 79, no. 1, pp. 103–113, 2011, doi: 10.1016/j.seppur.2011.03.024.

641　[23]　Q. Ping, B. Cohen, C. Dosoretz, and Z. He, "Long-term investigation of fouling of cation and
642　　　　anion exchange membranes in microbial desalination cells," *Desalination*, vol. 325, pp. 48–55,
643　　　　2013, doi: 10.1016/j.desal.2013.06.025.

644　[24]　S. Mikhaylin and L. Bazinet, "Fouling on ion-exchange membranes: Classification,
645　　　　characterization and strategies of prevention and control," *Adv. Colloid Interface Sci.*, vol. 229,
646　　　　no. December, pp. 34–56, 2016, doi: 10.1016/j.cis.2015.12.006.

647　[25]　J. Xu, G. P. Sheng, H. W. Luo, W. W. Li, L. F. Wang, and H. Q. Yu, "Fouling of proton
648　　　　exchange membrane (PEM) deteriorates the performance of microbial fuel cell," *Water Res.*,
649　　　　vol. 46, no. 6, pp. 1817–1824, 2012, doi: 10.1016/j.watres.2011.12.060.

650　[26]　Q. Xia *et al.*, "Study on the fouling mechanism and cleaning method in the treatment of polymer
651　　　　flooding produced water with ion exchange membranes," *RSC Adv.*, vol. 8, no. 52, pp. 29947–
652　　　　29957, 2018, doi: 10.1039/c8ra05575k.

653　[27]　S. Ramakrishna, K. Fujihara, W.-E. Teo, T.-C. Lim, and Z. Ma, *An Introduction to*
654　　　　*Electrospinning and Nanofibers*. WORLD SCIENTIFIC, 2005.

655　[28]　A. Greiner and J. H. Wendorff, "Electrospinning: A fascinating method for the preparation of
656　　　　ultrathin fibers," *Angew. Chemie - Int. Ed.*, vol. 46, no. 30, pp. 5670–5703, 2007, doi:
657　　　　10.1002/anie.200604646.

658　[29]　B. Swanckaert, J. Geltmeyer, K. Rabaey, K. De Buysser, L. Bonin, and K. De Clerck, "A review
659　　　　on ion-exchange nanofiber membranes: properties, structure and application in electrochemical
660　　　　(waste)water treatment," *Sep. Purif. Technol.*, vol. 287, 2022, doi:
661　　　　10.1016/j.seppur.2022.120529.

662　[30]　M. R. Bilad *et al.*, "Tackling membrane fouling in microalgae filtration using nylon 6,6 nanofiber
663　　　　membrane," *J. Environ. Manage.*, vol. 223, no. May, pp. 23–28, 2018, doi:
664　　　　10.1016/j.jenvman.2018.06.007.

665　[31]　M. A. Hammami *et al.*, "Engineering hydrophobic organosilica nanoparticle-doped nanofibers
666　　　　for enhanced and fouling resistant membrane distillation," *ACS Appl. Mater. Interfaces*, vol. 9,
667　　　　no. 2, pp. 1737–1745, 2017, doi: 10.1021/acsami.6b11167.

668　[32]　L. N. Nthunya *et al.*, "Fouling-resistant PVDF nanofibre membranes for the desalination of
669　　　　brackish water in membrane distillation," *Sep. Purif. Technol.*, vol. 228, no. March, p. 115793,
670　　　　2019, doi: 10.1016/j.seppur.2019.115793.

671　[33]　S. Zhang, A. Tanioka, and H. Matsumoto, "Nanofibers as novel platform for high-functional ion
672　　　　exchangers," *J. Chem. Technol. Biotechnol.*, vol. 93, no. 10, pp. 2791–2803, 2018, doi:
673　　　　10.1002/jctb.5685.

674　[34]　B. Dong, L. Gwee, D. Salas-De La Cruz, K. I. Winey, and Y. A. Elabd, "Super proton
675　　　　conductive high-purity nafion nanofibers," *Nano Lett.*, vol. 10, no. 9, pp. 3785–3790, 2010, doi:
676　　　　10.1021/nl102581w.

677　[35]　S. Imaizumi, H. Matsumoto, M. Ashizawa, M. Minagawa, and A. Tanioka, "Nanosize effects of

678   sulfonated carbon nanofiber fabrics for high capacity ion-exchanger," *RSC Adv.*, vol. 2, no. 7,
679   pp. 3109–3114, 2012, doi: 10.1039/c2ra20103h.

680 [36] M. Mann-Lahav *et al.*, "Electrospun Ionomeric Fibers with Anion Conducting Properties," *Adv.*
681   *Funct. Mater.*, vol. 30, no. 18, pp. 1–11, 2020, doi: 10.1002/adfm.201901733.

682 [37] R. Sood, S. Cavaliere, D. J. Jones, and J. Rozière, "Electrospun nanofibre composite polymer
683   electrolyte fuel cell and electrolysis membranes," *Nano Energy*, vol. 26, pp. 729–745, 2016,
684   doi: 10.1016/j.nanoen.2016.06.027.

685 [38] H. Wu, W. Pan, D. Lin, and H. Li, "Electrospinning of ceramic nanofibers: Fabrication,
686   assembly and applications," *J. Adv. Ceram.*, vol. 1, no. 1, pp. 2–23, 2012, doi: 10.1007/s40145-
687   012-0002-4.

688 [39] Z. Li, S. Liu, S. Song, W. Xu, Y. Sun, and Y. Dai, "Porous ceramic nanofibers as new catalysts
689   toward heterogeneous reactions," *Compos. Commun.*, vol. 15, no. July, pp. 168–178, 2019,
690   doi: 10.1016/j.coco.2019.07.004.

691 [40] D. Malwal and P. Gopinath, "Fabrication and applications of ceramic nanofibers in water
692   remediation: A review," *Crit. Rev. Environ. Sci. Technol.*, vol. 46, no. 5, pp. 500–534, 2016, doi:
693   10.1080/10643389.2015.1109913.

694 [41] D. Li, J. T. McCann, Y. Xia, and M. Marquez, "Electrospinning: A simple and versatile
695   technique for producing ceramic nanofibers and nanotubes," *J. Am. Ceram. Soc.*, vol. 89, no.
696   6, pp. 1861–1869, 2006, doi: 10.1111/j.1551-2916.2006.00989.x.

697 [42] Y. Liu, S. Sagi, R. Chandrasekar, L. Zhang, N. E. Hedin, and H. Fong, "Preparation and
698   characterization of electrospun SiO 2 nanofibers," *J. Nanosci. Nanotechnol.*, vol. 8, no. 3, pp.
699   1528–1536, 2008, doi: 10.1166/jnn.2008.043.

700 [43] S. W. Lee, Y. U. Kim, S. S. Choi, T. Y. Park, Y. L. Joo, and S. G. Lee, "Preparation of
701   SiO2/TiO2 composite fibers by sol-gel reaction and electrospinning," *Mater. Lett.*, vol. 61, no. 3,
702   pp. 889–893, 2007, doi: 10.1016/j.matlet.2006.06.020.

703 [44] J. Geltmeyer, L. Van Der Schueren, F. Goethals, K. De Buysser, and K. De Clerck, "Optimum
704   sol viscosity for stable electrospinning of silica nanofibres," *J. Sol-Gel Sci. Technol.*, vol. 67, no.
705   1, pp. 188–195, 2013, doi: 10.1007/s10971-013-3066-x.

706 [45] J. Geltmeyer, J. De Roo, F. Van den Broeck, J. C. Martins, K. De Buysser, and K. De Clerck,
707   "The influence of tetraethoxysilane sol preparation on the electrospinning of silica nanofibers,"
708   *J. Sol-Gel Sci. Technol.*, vol. 77, no. 2, pp. 453–462, 2016, doi: 10.1007/s10971-015-3875-1.

709 [46] E. Loccufier, J. Geltmeyer, L. Daelemans, D. R. D'hooge, K. De Buysser, and K. De Clerck,
710   "Silica Nanofibrous Membranes for the Separation of Heterogeneous Azeotropes," *Adv. Funct.*
711   *Mater.*, vol. 28, no. 44, pp. 1–10, 2018, doi: 10.1002/adfm.201804138.

712 [47] E. Cano-Serrano, J. M. Campos-Martin, and J. L. G. Fierro, "Sulfonic acid-functionalized silica
713   through quantitative oxidation of thiol groups," *Chem. Commun.*, no. 2, pp. 246–247, 2003, doi:
714   10.1039/b210766j.

715 [48] S. Choi and S. G. O. O. Lee, "Silica nanofibers from electrospinning/sol-gel process," *J. Mater.*
716   *Sci. Lett.*, vol. 22, pp. 891–893, 2003.

717 [49] K. Wilson, A. F. Lee, D. J. Macquarrie, and J. H. Clark, "Structure and reactivity of sol-gel
718   sulphonic acid silicas," *Appl. Catal. A Gen.*, vol. 228, no. 1–2, pp. 127–133, 2002, doi:
719   10.1016/S0926-860X(01)00956-5.

720 [50] S. J. Eichhorn and W. W. Sampson, "Relationships between specific surface area and pore
721   size in electrospun polymer fibre networks," *J. R. Soc. Interface*, vol. 7, no. 45, pp. 641–649,
722   2010, doi: 10.1098/rsif.2009.0374.

723 [51] J. Livage and C. Sanchez, "Sol-gel chemistry," *J. Non. Cryst. Solids*, vol. 145, no. C, pp. 11–
724   19, 1992, doi: 10.1016/S0022-3093(05)80422-3.

725 [52] C. A. Milea, C. Bogatu, and A. Duta, "The Influence of Parameters in Silica Sol-Gel Process,"
726   *Eng. Sci.*, vol. 4, no. 1, pp. 59–66, 2011.

727   [53]   T. Y. Chen and J. Leddy, "Ion exchange capacity of Nafion and Nafion composites," *Langmuir*,
728   vol. 16, no. 6, pp. 2866–2871, 2000, doi: 10.1021/la991094x.

729   [54]   M. I. San-Martín, F. J. Carmona, R. M. Alonso, P. Prádanos, A. Morán, and A. Escapa,
730   "Assessing the ageing process of cation exchange membranes in bioelectrochemical systems,"
731   *Int. J. Hydrogen Energy*, vol. 44, no. 47, pp. 25287–25296, 2019, doi:
732   10.1016/j.ijhydene.2019.08.004.

733   [55]   B. C. Smith, *Infrared spectral interpretation : a systematic approach*. Boca Raton (Fla.) : CRC
734   press, 1999.

735   [56]   D. Montes, J. Henao, E. A. Taborda, J. Gallego, F. B. Cortés, and C. A. Franco, "Effect of
736   Textural Properties and Surface Chemical Nature of Silica Nanoparticles from Different Silicon
737   Sources on the Viscosity Reduction of Heavy Crude Oil," *ACS Omega*, vol. 5, no. 10, pp.
738   5085–5097, 2020, doi: 10.1021/acsomega.9b04041.

739   [57]   F. Ghorban and A. Eshaghi, "Environmental effects on transparency and hydrophilicity of silica
740   nano-porous thin film coated glass substrates," *Opt. Quantum Electron.*, vol. 49, no. 2, pp. 1–
741   11, 2017, doi: 10.1007/s11082-017-0904-z.

742   [58]   A. Luqman, O. Aderemi, G. Tony, M. Hylton, and L. Zhiping, "Preparation and Characterization
743   of Sulfonic Acid functionalized single-walled Carbon Nanotubes," *Phys. E Low-Dimensional
744   Syst. Nanostructures*, vol. 41, no. 4, pp. 723–728, 2009.

745   [59]   M. Kageyama *et al.*, "Surface Modification of Self-assembled Monolayers of Thiol- and
746   Disulfide-terminated Organosilanes by UV/ozone Treatment toward Fabrication of Damaged-
747   Hair Surface Models," *Trans. Mater. Res. Soc. Japan*, vol. 39, no. 1, pp. 61–65, 2014, doi:
748   10.14723/tmrsj.39.61.

749   [60]   W. J. Eakins, "Silanol groups on silica and their reactions with trimethyl chlorosilane and
750   trimethylsilanol," *Ind. Eng. Chem. Prod. Res. Dev.*, vol. 7, no. 1, pp. 39–43, 1968, doi:
751   10.1021/i360025a009.

752   [61]   M. L. Hair and W. Hertl, "Reactions of chlorosilanes with silica surfaces," *J. Phys. Chem.*, vol.
753   73, no. 7, pp. 2372–2378, 1969, doi: 10.1021/j100727a046.

754   [62]   A. A. Jalali, F. Mohammadi, and S. N. Ashrafizadeh, "Effects of process conditions on cell
755   voltage, current efficiency and voltage balance of a chlor-alkali membrane cell," *Desalination*,
756   vol. 237, no. 1–3, pp. 126–139, 2009, doi: 10.1016/j.desal.2007.11.056.

757   [63]   M. M. Rashid, M. K. Al Mesfer, H. Naseem, and M. Danish, "Hydrogen Production by Water
758   Electrolysis: A Review of Alkaline Water Electrolysis, PEM Water Electrolysis and High
759   Temperature Water Electrolysis," *Int. J. Eng. Adv. Technol.*, no. 3, pp. 2249–8958, 2015.

760   [64]   A. Hauch, S. D. Ebbesen, S. H. Jensen, and M. Mogensen, "Highly efficient high temperature
761   electrolysis," *J. Mater. Chem.*, vol. 18, no. 20, pp. 2331–2340, 2008, doi: 10.1039/b718822f.

762   [65]   T. Ueda, K. Wakitani, and A. Nanasawa, "Influence of electrolyte temperature on efficiency of
763   electrochemical chloride removal from concrete," *Electrochim. Acta*, vol. 86, pp. 23–27, 2012,
764   doi: 10.1016/j.electacta.2012.05.026.

765   [66]   S. Ek, A. Root, M. Peussa, and L. Niinistö, "Determination of the hydroxyl group content in
766   silica by thermogravimetry and a comparison with 1H MAS NMR results," *Thermochim. Acta*,
767   vol. 379, no. 1–2, pp. 201–212, 2001, doi: 10.1016/S0040-6031(01)00618-9.

768   [67]   J. Gi Hong and Y. Chen, "Evaluation of electrochemical properties and reverse electrodialysis
769   performance for porous cation exchange membranes with sulfate-functionalized iron oxide," *J.
770   Memb. Sci.*, vol. 473, pp. 210–217, 2015, doi: 10.1016/j.memsci.2014.09.012.

771   [68]   C. Klaysom, S. H. Moon, B. P. Ladewig, G. Q. M. Lu, and L. Wang, "Preparation of porous ion-
772   exchange membranes (IEMs) and their characterizations," *J. Memb. Sci.*, vol. 371, no. 1–2, pp.
773   37–44, 2011, doi: 10.1016/j.memsci.2011.01.008.

774   [69]   N. Gizli, S. Çinarli, and M. Demircioglu, "Characterization of poly(vinylchloride) (PVC) based
775   cation exchange membranes prepared with ionic liquid," *Sep. Purif. Technol.*, vol. 97, pp. 96–

776   107, 2012, doi: 10.1016/j.seppur.2012.02.028.

777 [70] D. T. M. Huong, B. L. Liu, W. S. Chai, P. L. Show, S. L. Tsai, and Y. K. Chang, "Highly efficient
778   dye removal and lysozyme purification using strong and weak cation-exchange nanofiber
779   membranes," *Int. J. Biol. Macromol.*, vol. 165, pp. 1410–1421, 2020, doi:
780   10.1016/j.ijbiomac.2020.10.034.

781 [71] H. Matsumoto, Y. Wakamatsu, M. Minagawa, and A. Tanioka, "Preparation of ion-exchange
782   fiber fabrics by electrospray deposition," *J. Colloid Interface Sci.*, vol. 293, no. 1, pp. 143–150,
783   2006, doi: 10.1016/j.jcis.2005.06.022.

784 [72] R. Moreno-Cervera, M. Aguilar-Vega, J. Domínguez-Maldonado, G. Cámara-Chale, and L.
785   Alzate-Gaviria, "Performance of a greywater cathode in a microbial fuel cell with three ion
786   exchange membranes," *J. Chem. Technol. Biotechnol.*, vol. 94, no. 5, pp. 1601–1612, 2019,
787   doi: 10.1002/jctb.5927.

788 [73] A. Sotres *et al.*, "Microbial community dynamics in two-chambered microbial fuel cells: Effect of
789   different ion exchange membranes," *J. Chem. Technol. Biotechnol.*, vol. 90, no. 8, pp. 1497–
790   1506, 2015, doi: 10.1002/jctb.4465.

791 [74] M. Greiter, S. Novalin, M. Wendland, K. D. Kulbe, and J. Fischer, "Electrodialysis versus ion
792   exchange: Comparison of the cumulative energy demand by means of two applications," *J.
793   Memb. Sci.*, vol. 233, no. 1–2, pp. 11–19, 2004, doi: 10.1016/j.memsci.2003.11.027.

794 [75] X. Y. Nie, S. Y. Sun, Z. Sun, X. Song, and J. G. Yu, "Ion-fractionation of lithium ions from
795   magnesium ions by electrodialysis using monovalent selective ion-exchange membranes,"
796   *Desalination*, vol. 403, pp. 128–135, 2017, doi: 10.1016/j.desal.2016.05.010.

797 [76] I. Sas, R. E. Gorga, J. A. Joines, and K. A. Thoney, "Literature review on superhydrophobic
798   self-cleaning surfaces produced by electrospinning," *J. Polym. Sci. Part B Polym. Phys.*, vol.
799   50, no. 12, pp. 824–845, 2012, doi: 10.1002/polb.23070.

800 [77] N. Nuraje, W. S. Khan, Y. Lei, M. Ceylan, and R. Asmatulu, "Superhydrophobic electrospun
801   nanofibers," *J. Mater. Chem. A*, vol. 1, no. 6, pp. 1929–1946, 2013, doi: 10.1039/c2ta00189f.

802 [78] B. J. Teppen and D. M. Miller, "Hydration Energy Determines Isovalent Cation Exchange
803   Selectivity by Clay Minerals," *Soil Sci. Soc. Am. J.*, vol. 70, no. 1, pp. 31–40, 2006, doi:
804   10.2136/sssaj2004.0212.

805 [79] E. R. Nightingale, "Phenomenological theory of ion solvation. Effective radii of hydrated ions,"
806   *J. Phys. Chem.*, vol. 63, no. 9, pp. 1381–1387, 1959, doi: 10.1021/j150579a011.

807 [80] Q. B. Chen, Z. Y. Ji, J. Liu, Y. Y. Zhao, S. Z. Wang, and J. S. Yuan, "Development of
808   recovering lithium from brines by selective-electrodialysis: Effect of coexisting cations on the
809   migration of lithium," *J. Memb. Sci.*, vol. 548, no. 8, pp. 408–420, 2018, doi:
810   10.1016/j.memsci.2017.11.040.

811 [81] G. Eisenman and R. Horn, "Ionic selectivity revisited: The role of kinetic and equilibrium
812   processes in ion permeation through channels," *J. Membr. Biol.*, vol. 76, no. 3, pp. 197–225,
813   1983, doi: 10.1007/BF01870364.

814 [82] B. Tansel, "Significance of thermodynamic and physical characteristics on permeation of ions
815   during membrane separation: Hydrated radius, hydration free energy and viscous effects," *Sep.
816   Purif. Technol.*, vol. 86, pp. 119–126, 2012, doi: 10.1016/j.seppur.2011.10.033.

817 [83] H. Strathmann, *Chapter 6 Ion-Exchange Membrane Processes in Water Treatment*, vol. 2, no.
818   C. Elsevier, 2010.

819 [84] Y. H. Li, Y. Z. Yu, J. H. Qian, H. A. Wu, and F. C. Wang, "Anomalous ion transport through
820   angstrom-scale pores: Effect of hydration shell exchange on ion mobility," *Appl. Surf. Sci.*, vol.
821   560, no. February, p. 150022, 2021, doi: 10.1016/j.apsusc.2021.150022.

822 [85] S. Koneshan, J. C. Rasaiah, R. M. Lynden-Bell, and S. H. Lee, "Solvent structure, dynamics,
823   and ion mobility in aqueous solutions at 25 °C," *J. Phys. Chem. B*, vol. 102, no. 21, pp. 4193–
824   4204, 1998, doi: 10.1021/jp980642x.

825   [86]   G. B. Alexander, W. M. Heston, and R. K. Iler, "The Solubility of Amorphous Silica in Water," *J.*
826   *Phys. Chem.*, vol. 58, no. 6, pp. 453–455, Jun. 1954, doi: 10.1021/j150516a002.

827   [87]   R. Ghalloussi, L. Chaabane, C. Larchet, L. Dammak, and D. Grande, "Structural and
828   physicochemical investigation of ageing of ion-exchange membranes in electrodialysis for food
829   industry," *Sep. Purif. Technol.*, vol. 123, pp. 229–234, 2014, doi: 10.1016/j.seppur.2013.12.020.

830   [88]   R. Ghalloussi *et al.*, "Ageing of ion-exchange membranes used in electrodialysis: Investigation
831   of static parameters, electrolyte permeability and tensile strength," *Sep. Purif. Technol.*, vol. 80,
832   no. 2, pp. 270–275, 2011, doi: 10.1016/j.seppur.2011.05.005.

833   [89]   X. Tong, B. Zhang, and Y. Chen, "Fouling resistant nanocomposite cation exchange membrane
834   with enhanced power generation for reverse electrodialysis," *J. Memb. Sci.*, vol. 516, pp. 162–
835   171, 2016, doi: 10.1016/j.memsci.2016.05.060.

836   [90]   C. Casademont, G. Pourcelly, and L. Bazinet, "Effect of magnesium/calcium ratio in solutions
837   subjected to electrodialysis: Characterization of cation-exchange membrane fouling," *J. Colloid*
838   *Interface Sci.*, vol. 315, no. 2, pp. 544–554, 2007, doi: 10.1016/j.jcis.2007.06.056.

839   [91]   W. C. Cheong, P. H. Gaskell, and A. Neville, "Substrate effect on surface
840   adhesion/crystallisation of calcium carbonate," *J. Cryst. Growth*, vol. 363, pp. 7–21, 2013, doi:
841   10.1016/j.jcrysgro.2012.09.025.

842